

# Drake Antarctic Agile Meteor Radar first results: Configuration and comparison of mean and tidal wind and gravity wave momentum flux measurements with Southern Argentina Agile Meteor Radar

D. C. Fritts,<sup>1</sup> D. Janches,<sup>2</sup> H. Iimura,<sup>1</sup> W. K. Hocking,<sup>3</sup> J. V. Bageston,<sup>4</sup> and N. M. P. Leme<sup>4</sup>

Received 29 July 2011; revised 2 November 2011; accepted 12 November 2011; published 21 January 2012.

[1] A new generation meteor radar was installed at the Brazilian Antarctic Comandante Ferraz Base (62.1°S) in March 2010. This paper describes the motivations for the radar location, its measurement capabilities, and comparisons of measured mean winds, tides, and gravity wave momentum fluxes from April to June of 2010 and 2011 with those by a similar radar on Tierra del Fuego (53.8°S). Motivations for the radars include the “hotspot” of small-scale gravity wave activity extending from the troposphere into the mesosphere and lower thermosphere (MLT) centered over the Drake Passage, the maximum of the semidiurnal tide at these latitudes, and the lack of other MLT wind measurements in this latitude band. Mean winds are seen to be strongly modulated at planetary wave and longer periods and to exhibit strong coherence over the two radars at shorter time scales as well as systematic seasonal variations. The semidiurnal tide contributes most to the large-scale winds over both radars, with maximum tidal amplitudes during May and maxima at the highest altitudes varying from  $\sim 20$  to  $>70$   $\text{ms}^{-1}$ . In contrast, the diurnal tide and various planetary waves achieve maximum winds of  $\sim 10$  to  $20$   $\text{ms}^{-1}$ . Monthly mean gravity wave momentum fluxes appear to reflect the occurrence of significant sources at lower altitudes, with relatively small zonal fluxes over both radars, but with significant, and opposite, meridional momentum fluxes below  $\sim 85$  km. These suggest gravity waves propagating away from the Drake Passage at both sites, and may indicate an important source region accounting in part for this “hotspot.”

**Citation:** Fritts, D. C., D. Janches, H. Iimura, W. K. Hocking, J. V. Bageston, and N. M. P. Leme (2012), Drake Antarctic Agile Meteor Radar first results: Configuration and comparison of mean and tidal wind and gravity wave momentum flux measurements with Southern Argentina Agile Meteor Radar, *J. Geophys. Res.*, 117, D02105, doi:10.1029/2011JD016651.

## 1. Introduction

[2] It is now well known that the structure and variability of the mesosphere and lower thermosphere (MLT) is determined to a significant degree by large- and small-scale waves propagating into this region from below. Tides, planetary waves (PWs), and gravity waves (GWs) exhibit significant variability with season and latitude due to seasonal variations in their sources and propagation environments [e.g., Holton, 1984; Burrage *et al.*, 1995; Vincent *et al.*, 1998; Manson *et al.*, 1999; Pancheva *et al.*, 2002, 2004, 2009; McLandress, 2002; Fritts and Alexander, 2003; Lieberman

*et al.*, 2004; Murphy *et al.*, 2006]. GWs and tides also exhibit longitudinal variability reflecting the longitudinal distributions of their forcing dynamics [e.g., Tsuda *et al.*, 2000; Hagan and Forbes, 2002, 2003; Espy *et al.*, 2006]. Indeed, there are preferred latitudes and longitudes where these various motions systematically achieve their largest responses. Possibly the most dramatic responses, and potential for interactions among large- and small-scale motions, occur in late fall and winter at middle to high latitudes. Semidiurnal tide and PW winds maximize here [Forbes, 1995; Hagan and Forbes, 2003], and GWs exhibit strong responses at lower altitudes over specific source regions [McLandress *et al.*, 2000; Ern *et al.*, 2004; Wu, 2004; Jiang *et al.*, 2006; Alexander *et al.*, 2008a; Wu and Eckermann, 2008] that clearly extend into the MLT in some cases. Most of these apparent GW source regions in both hemispheres correlate with high terrain. Of these, the region encompassing the Andes, the Drake Passage, and the Antarctic Peninsula appears to exhibit the largest responses on Earth [Jiang *et al.*, 2002; Preusse *et al.*, 2002, 2006; Wu and Jiang, 2002; Eckermann *et al.*, 2006; Wu *et al.*, 2006; Alexander *et al.*, 2008b; Hertzog *et al.*, 2008]. Indeed, this region has

<sup>1</sup>Colorado Research Associates Division, NorthWest Research Associates, Boulder, Colorado, USA.

<sup>2</sup>Space Weather Laboratory, NASA Goddard Space Flight Center, Greenbelt, Maryland, USA.

<sup>3</sup>Department of Physics, University of Western Ontario, London, Ontario, Canada.

<sup>4</sup>Instituto Nacional de Pesquisas Espaciais, São José dos Campos, Brazil.

yielded a number of examples of strong interactions among these various motions, despite limited observational capabilities until recently [Smith *et al.*, 2009; Beldon and Mitchell, 2010; Fritts *et al.*, 2010a, 2010b].

[3] The large amplitudes anticipated for the various tidal, PW, and GW motions in the Drake Passage “hotspot,” and our expectation for strong interactions among these various motions, were the motivations for placing two new generation meteor radars in the northern and southern portions of this natural laboratory for MLT dynamics studies. The Southern Argentina Agile Meteor Radar (SAAMER) was installed at Rio Grande on Tierra del Fuego (53.8°S, 67.8°W) in May 2008, and a nearly identical system, the Drake Antarctic Agile Meteor Radar (DrAAMER), was installed at the Brazilian Antarctic Comandante Ferraz Base (62.1°S, 58.7°W) in March 2010. The two radars were specifically designed to measure both the large-scale (mean, tidal, and PW) motion fields with high precision and the vertical fluxes of horizontal momentum by GWs, the latter of which previously has only been possible with significantly larger and more expensive radars and lidars. SAAMER capabilities for mean, tidal, and PW wind measurements were demonstrated by Fritts *et al.* [2010a, 2011, hereafter F10a and F11]. The potential for GW momentum flux measurements was evaluated and first employed using SAAMER by Fritts *et al.* [2010b, hereafter F10b].

[4] An additional capability that we hope will be demonstrated with these radars with further analysis is the potential to measure GW-tidal and GW-PW interactions and their modulation of GW variances and momentum fluxes. Such interactions have been observed in limited MLT observations [Fritts and Vincent, 1987; Wang and Fritts, 1991; Thayaparan *et al.*, 1995; Isler and Fritts, 1996; Manson *et al.*, 1998; Murphy and Vincent, 1998; Preusse *et al.*, 2001; Espy *et al.*, 2004; Beldon and Mitchell, 2010] and in numerical models of these dynamics [Holton, 1984; Miyahara 1985; Miyahara *et al.*, 1986; Forbes *et al.*, 1991; Lu and Fritts, 1993; Eckermann and Marks, 1996; Meyer, 1999; Ortland and Alexander, 2006; Liu *et al.*, 2008]. They have yet to be fully quantified, understood, and adequately parameterized in large-scale models, however [McLandress and Ward, 1994; McLandress, 1998, 2002; Hagan *et al.*, 1999; Fritts and Alexander, 2003], hence such measurements where these interaction dynamics are particularly strong would prove valuable in constraining such efforts.

[5] Our purposes in this paper are to describe the DrAAMER radar system and compare its measurement capabilities for large- and small-scale MLT dynamics with those of SAAMER for April, May, and June of its first 2 years of operation. The radar configuration, the spatial and temporal variations of meteor detections observed from Ferraz, and our data analysis methods are described in section 2. DrAAMER mean and tidal winds during April, May, and June of 2010 and 2011 are described and compared with those measured by SAAMER from 2009 to 2011 and with the Global-Scale Wave Model, version 2009 (GSWM-09 [see Zhang *et al.*, 2010a, 2010b]) in sections 3 and 4. Section 5 compares monthly mean GW momentum fluxes estimated by DrAAMER and SAAMER during April, May, and June 2010 and 2011. A discussion of these results and our summary and conclusions are provided in sections 6 and 7. A separate assessment by D. C. Fritts *et al.* (Assessment of

gravity wave momentum flux measurement capabilities by meteor radars having different transmitter power and antenna configurations, submitted to the *Journal of Geophysical Research*, 2011) of DrAAMER GW momentum flux measurement capabilities compared to SAAMER and three other meteor radars explores the potential for similar measurements with traditional meteor radars.

## 2. DrAAMER System Description and Data Analysis

### 2.1. System Description

[6] Like SAAMER (F10a, F10b), DrAAMER was specifically configured to enable high-resolution definition of the large-scale wind field and potential sensitivity to GW momentum fluxes employing a generalization of the dual-beam technique first employed by Vincent and Reid [1983] and extended to multiple-beam studies by VanZandt *et al.* [1990] and Fritts *et al.* [1990]. Definition of both the large-scale motion field at high resolution and GW momentum fluxes requires high meteor count rates at sufficiently small off-zenith angles to allow vertical motions due to GWs to make significant contributions to the inferred radial velocities. As with SAAMER, this was accomplished through significantly higher peak power than employed by typical meteor radars and a transmitting array that directs the majority of radar power into eight beams at 45° azimuth increments with peak power at ~35° off zenith. This results in a majority of meteor detections at off-zenith angles between 15° and 50°. The SAAMER and DrAAMER antenna patterns, daily counts, and altitude distributions of accepted meteors are illustrated for 1 day in Figure 1 (top) and for April, May, and June 2011 Figure 1 (bottom) (note the log scale at lower left). All-sky unambiguous meteor detections achieving a threshold accuracy (~50% of the totals) average ~19,800 and ~8500 per day at SAAMER and DrAAMER, respectively.

[7] DrAAMER radar parameters and measurement capabilities include (1) a radar frequency of 36.9 MHz and bandwidths ranging from 35 to 125 kHz; (2) a peak transmitter power of 30 kW; (3) a transmitter antenna composed of eight three-element crossed Yagis in a circle of diameter 24.4 m having opposite phasing of every other Yagi (normal mode); (4) five receiver channels to reduce meteor position ambiguities [Jones *et al.*, 1998]; (5) a transmit/receive (T/R) switch allowing both tropospheric measurements and use of the transmitter antenna as a sixth receiver; (6) a transmitter phasing option that allows power to be directed vertically; (7) various pulse coding, pulse repetition frequency (PRF), and integration options; and (8) sufficient power and beam definition flexibility to perform enhanced meteoroid radiant, population size, and “head echo” studies normally possible only with high-power, large-aperture (HPLA) radars. Since commissioning, DrAAMER has employed a 2-bit code, a PRF of 1730 Hz, integration over four samples, and meteor sampling at altitudes from 70 to 110 km.

### 2.2. Data Analysis

[8] Mean and tidal winds are obtained from hourly mean zonal and meridional winds in 3 km altitude bins from ~78 to 99 km employing radial velocities at off-zenith angles between 15 and 50°. These estimates include ~50 and

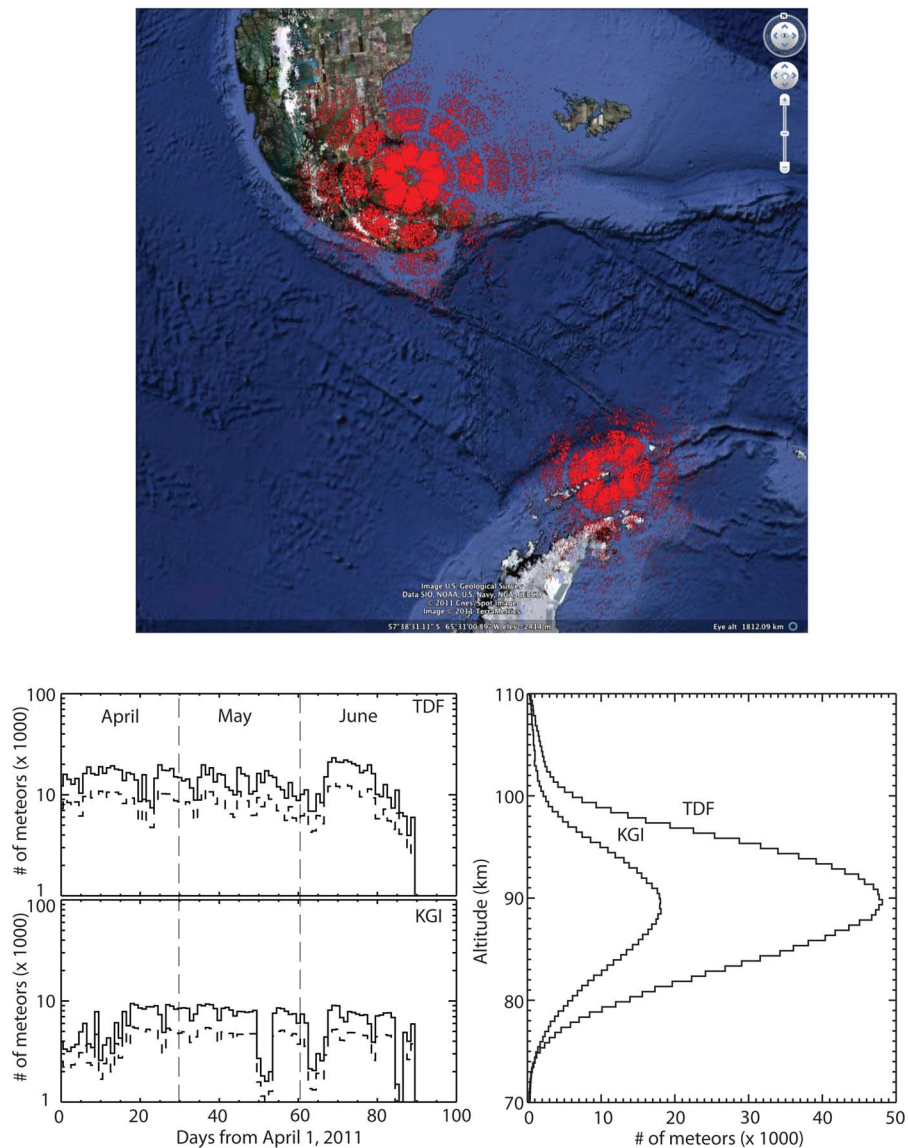


**Figure 1.** (top) Unambiguous meteors detected by SAAMER (on Tierra del Fuego) and DrAAMER (on King George Island) for 1 day showing the radar beam sensitivity. (bottom left) Daily unambiguous meteor counts over (top) SAAMER/TdF during 2011 and (bottom) DrAAMER/KGI, and (bottom right) meteor altitude distributions over each radar for April to June 2011. Solid and dashed lines at lower left show all meteors and meteors between  $15^\circ$  and  $50^\circ$  zenith angles, respectively. Google Earth imagery © Google Inc. Used with permission.

100 meteors/h near 90 km on average over DrAAMER and SAAMER, respectively, and a minimum of 5 meteors/h is required for a valid horizontal wind estimate at the higher and lower altitudes. Daily mean zonal and meridional winds and diurnal and semidiurnal tide amplitudes are determined employing a continuous “S-transform” [Stockwell *et al.*, 1996] Gaussian wavelet analysis applied to the hourly mean winds. Monthly mean winds and tidal amplitudes are computed for 2010 and 2011 from daily means for which a minimum of 12 hourly mean wind estimates are available, with missing daily means interpolated from third-order spline fits. We present daily mean winds and tides over DrAAMER only for 2011, however, due to five  $\sim 3$  to 10 day intervals during May and June 2010 for which no data were obtained.

Zonal and meridional wind spectra spanning the 3 month analysis period during 2011 are computed from the hourly mean winds at 90 km.

[9] Meteor radial velocity magnitudes larger than  $(20 + 3 A_z) \text{ ms}^{-1}$  (where  $A_z$  is the meteor zenith angle in degrees) are considered too large to be realistic for the maximum mean winds and tidal and GW amplitudes anticipated. We also display mean and tidal amplitudes at the highest altitudes only where these results exhibit reasonable amplitude growth with altitude.

[10] Monthly GW momentum fluxes are estimated using the method of Hocking [2005] following removal of mean and tidal winds derived from “S transform” fits to the hourly mean winds. S transform means and tidal amplitudes

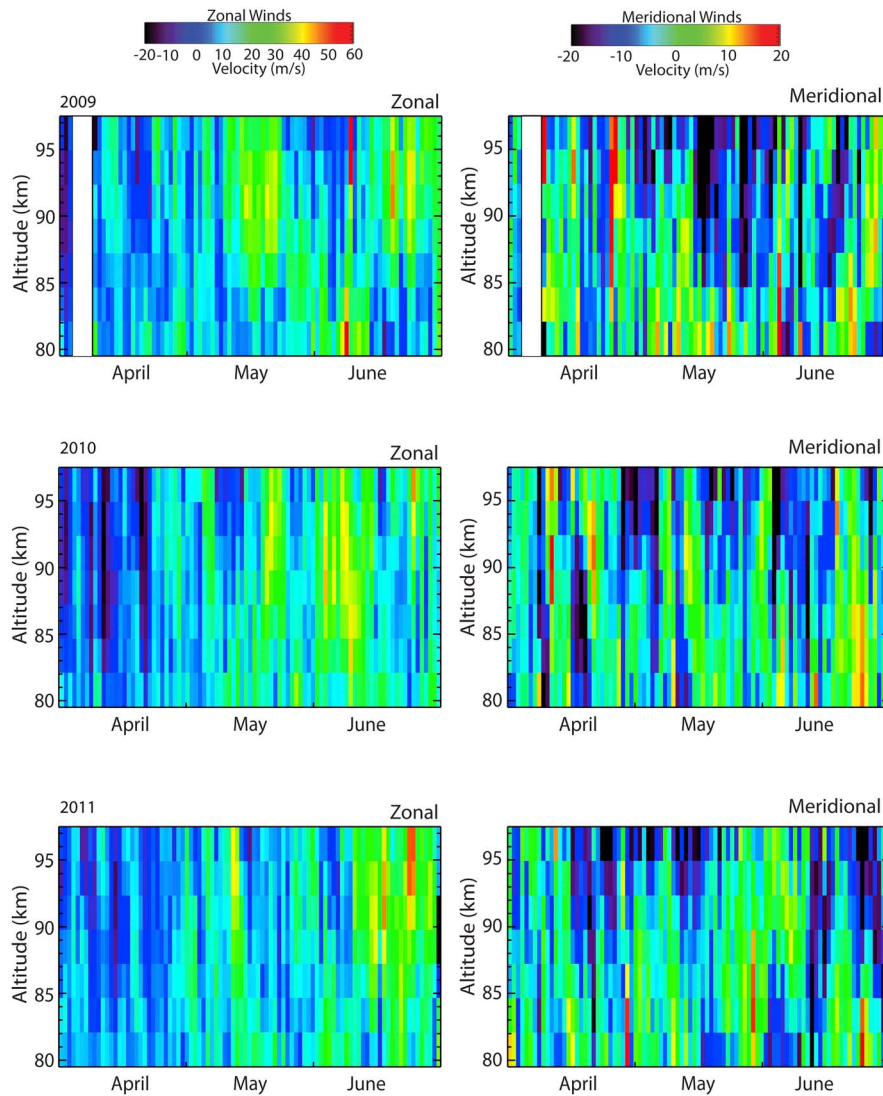


**Figure 2.** (left) Zonal and (right) meridional daily mean winds over SAAMER for April, May, and June of (top) 2009, (middle) 2010, and (bottom) 2011. Note the difference color scales in each column. Missing data are shown as white.

employed for these assessments allow more complete removal of varying mean and tidal motions in the presence of data gaps, as seen in the DrAAMER data in Figure 1. A three-point triangular smoothing is used to reduce estimation uncertainties. Such monthly momentum flux assessments were evaluated extensively by F10b and found to yield reasonable estimates for a wide range of test fields employing SAAMER.

### 3. Mean Winds and Spectra

[11] We present here daily mean and monthly mean winds, and their S transforms, over DrAAMER and SAAMER to illustrate their similarities and differences on daily to interannual time scales. Daily mean winds over SAAMER are displayed for April, May, and June of 2009, 2010, and 2011 (top to bottom) in Figure 2. Daily mean winds over DrAAMER for April, May, and June 2011 are shown for comparison in Figure 3 (top). Corresponding S transforms of

the zonal and meridional daily mean winds at 96 km over SAAMER for April, May, and June of each year are shown in Figures 4a–4c and Figures 4e–4g. S transforms of zonal and meridional daily mean winds at 96 km over DrAAMER for April, May, and June 2011 are shown in Figures 4d and 4h. Monthly mean winds over the two radars are shown for April (Figure 5, top), May (Figure 5, middle), and June (Figure 5, bottom) of 2010 and 2011. Spectra of hourly mean zonal and meridional winds at 88.5 km over DrAAMER from April to June 2011 are shown for periods from 2 h to  $\sim 40$  days in Figure 6 (top and bottom), respectively.

[12] Daily mean winds over SAAMER during 2009, 2010, and 2011 reveal similar seasonal trends each year, with weak westward or eastward mean winds during April and increasingly eastward mean winds arising during May and June at all altitudes. Westward maxima approach  $\sim 20 \text{ ms}^{-1}$  in April, while eastward maxima reaching  $\sim 50 \text{ ms}^{-1}$  become much more prevalent in May and June of each year. Meridional wind maxima vary from  $\sim -30$  to  $30 \text{ ms}^{-1}$  throughout

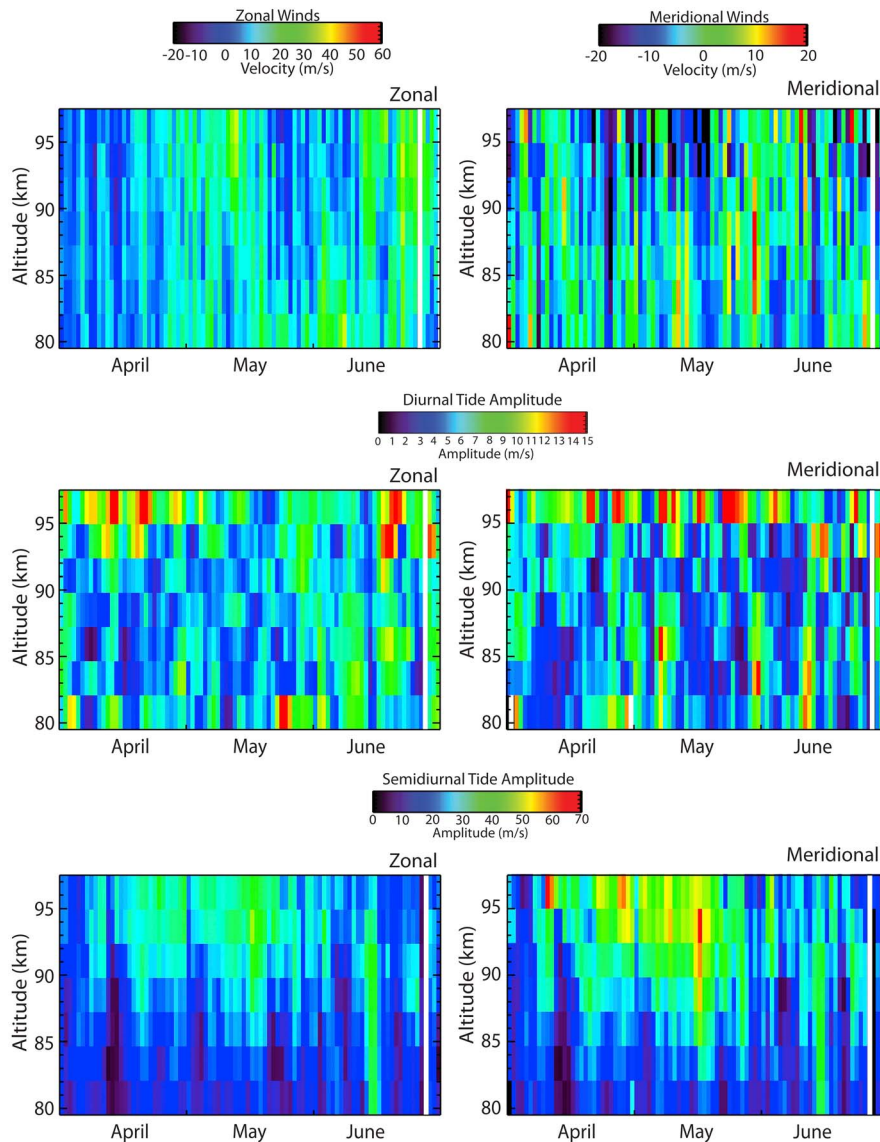


**Figure 3.** (left) Zonal and (right) meridional (top) daily mean winds, (middle) diurnal tide amplitudes, and (bottom) semidiurnal tide amplitudes over DrAAMER for April, May, and June of 2011. Note the difference color scales in each row. Missing data are shown as white.

these 3 months each year. PWs and longer-period oscillations ranging from periods of  $\sim 2$  to 40 days or longer are seen to occur each year and to contribute to the maximum zonal and meridional winds throughout each interval. As described by F11, the PWs observed over SAAMER having periods from  $\sim 8$  to 20 days exhibit significant temporal variability and a range of phase relationships among the wind components, suggesting strong transience and interactions among the various PW and tidal motions. In particular, inspection of Figure 2 indicates that the broader eastward wind maxima appear to correlate most strongly with southward meridional winds each year (see the eastward maxima centered in mid May 2009, mid to late May and early and late June of 2010, and mid May and late June 2011). Mean winds over DrAAMER during 2011 (Figure 3, top) closely resemble those over SAAMER throughout these three months, indicating that the spatial scales of the mean winds and the PW

and longer-period oscillations are significantly greater than the separation between the two radars.

[13] Longer-period oscillations were not addressed by F11, but were seen to occur in the S transforms of the mean winds in Figure 3 of that study. S transforms of the mean winds displayed in Figure 4 exhibit the relative contributions of PWs and longer-period oscillations to the zonal and meridional winds throughout each season over SAAMER and for 2011 over DrAAMER. Over SAAMER, significant modulations of the mean winds occur at periods from  $\sim 5$  to 40 days, with the most prevalent oscillations of  $\sim 5$  to 10 day periods throughout 2009 and 2010 and primarily during June of 2011,  $\sim 15$  to 20 day periods from April into May 2009, from late April into June 2010, and during May and June 2011, and  $\sim 30$  to 45 day periods contributing throughout 2009 and primarily during June of 2010 and 2011, respectively. SAAMER and DrAAMER mean wind S transforms

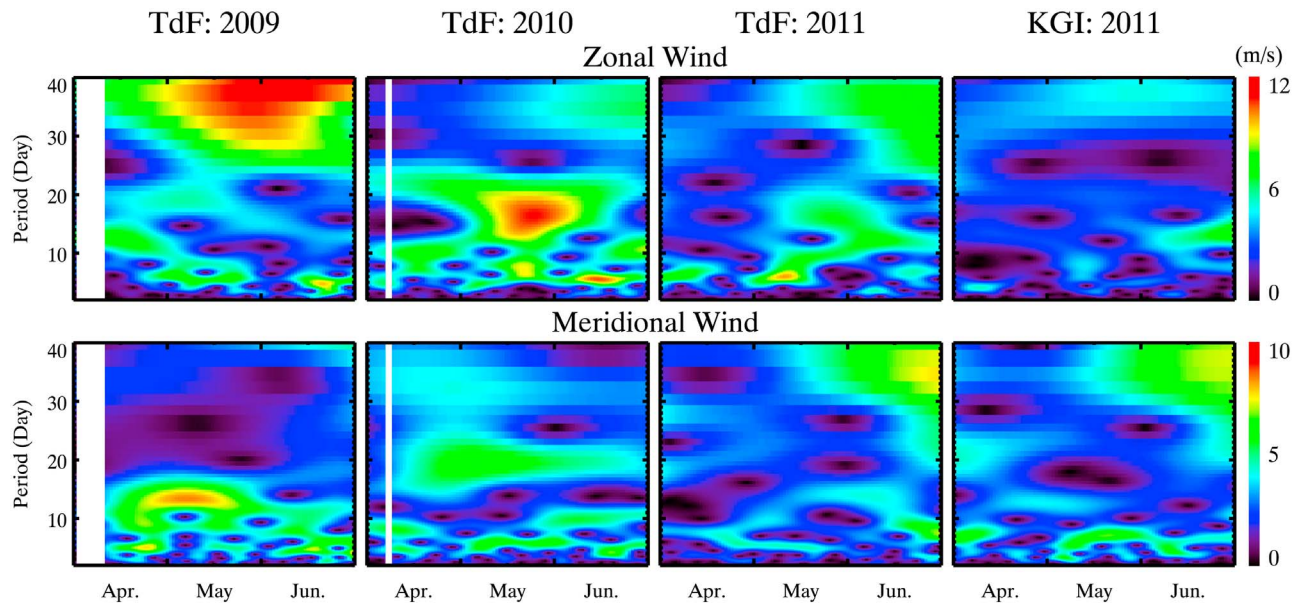


**Figure 4.** S transforms of (top) zonal and (bottom) meridional daily mean winds at 96 km for April, May, and June (left to right) of 2009, 2010, and 2011, respectively, over SAAMER and for 2011 over DrAAMER at 96 km. Amplitudes at each frequency are shown with the color bars at right. Missing data are shown as white.

for 2011 exhibit some similarities, but also clear differences, at  $\sim 5$  to 15 day periods throughout, with very strong correlations in their temporal variability largely in late May and June at periods of  $\sim 20$  days and longer.

[14] Monthly mean zonal and meridional winds over DrAAMER and SAAMER (red and blue, respectively) are compared for 2010 and 2011 (solid and dashed, respectively) in Figure 5. Monthly mean zonal winds in April are weak and eastward in all cases ( $\sim 10 \text{ ms}^{-1}$  or less), despite the sporadic negative excursions seen to accompany PW and longer-period oscillations in Figures 2 and 3. Mean zonal winds increase by  $\sim 5$  to  $10 \text{ ms}^{-1}$  from April to May, with somewhat larger increases in 2010 and over SAAMER compared to DrAAMER. Mean zonal winds increase again by  $\sim 5$  to  $10 \text{ ms}^{-1}$  from May to June over SAAMER, with the larger increases at middle and higher altitudes. DrAAMER mean zonal winds, however, increase very little from May to June, with the largest changes below  $\sim 90$  km in 2011.

[15] Monthly mean meridional winds during both 2010 and 2011 in all three months remain between  $\sim -5$  and  $5 \text{ ms}^{-1}$ , except over SAAMER, and over DrAAMER in May 2011, at the higher altitudes. Note that monthly mean winds are not displayed over DrAAMER above 96 km for several months due to a lack of sufficient meteor detections to satisfy our measurement constraints. While mean meridional winds over both radars during June 2010 below  $\sim 90$  km are equatorward rather than poleward (as expected to result from GW driving of the residual circulation and implying subsidence in the winter polar mesosphere), there are several factors that may account for this behavior. As noted by F10b, the winter jet in June over SAAMER typically extends to higher altitudes, with a weaker (poleward, as seen) residual circulation at even higher altitudes, than seen at other sites. This response may be linked to unusual GW forcing of the MLT over the Drake Passage “hotspot” (see F10b) that will be

discussed further below. There is also considerable variability imposed by PWs and longer-period oscillations that may influence estimates of monthly mean meridional motions at the level of the variations seen to occur in Figure 5.

[16] Spectra of hourly mean zonal and meridional velocities centered at 88.5 km over DrAAMER spanning periods from 2 h to  $\sim 40$  days are shown in Figures 6 (top and bottom), respectively. These spectra closely resemble those obtained over SAAMER by F10a, with maximum power in the semidiurnal tide, a clear but weaker diurnal peak, and distinct terdiurnal peaks. Also seen is an apparent continuum of GW motions at periods shorter than the inertial period at the DrAAMER latitude ( $\sim 13.6$  h), a sharper apparent decrease in spectral power near the inertial period than seen over SAAMER, and evidence of PW variance enhancements at longer periods than the diurnal tide, with comparable variances in the zonal and meridional components at periods from  $\sim 1$  to 10 days and somewhat larger zonal variances at longer periods. We note also that GW variances are likely greater than implied by these spectra because the hourly fits to the meteor winds from which the spectra were computed do not capture GW structures having significant horizontal phase variations across the central radar beams extending to  $50^\circ$  off-zenith, corresponding to a  $\sim 140$  km horizontal averaging at 90 km altitude.

## 4. Tidal Winds

### 4.1. Diurnal Tide

[17] Time-height cross sections of daily diurnal tide zonal and meridional wind amplitudes over DrAAMER during April, May, and June 2011 are displayed in the second panels of Figure 3. Monthly mean diurnal tide amplitudes and phases over DrAAMER and SAAMER (red and blue, respectively) are shown together for April (Figure 7, top),

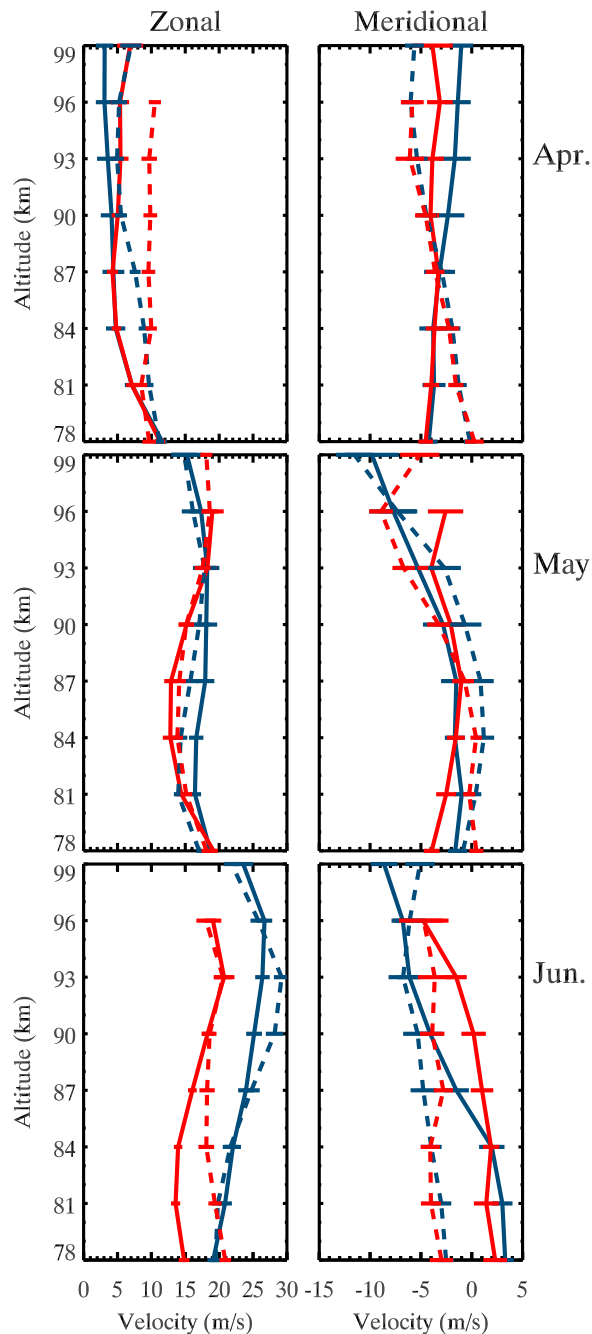


**Figure 5.** Monthly mean (left) zonal and (right) meridional winds for (top) April, (middle) May, and (bottom) June of 2010 (solid lines) and 2011 (dashed lines) over DrAAMER (red) and SAAMER (blue). Standard deviations are shown with horizontal lines in each case.

May (Figure 7, middle), and June (Figure 7, bottom). Zonal and meridional components are shown in Figures 7 (left) and 7 (right), and results for 2010 and 2011 are shown with solid and dashed lines, respectively. Black lines in each panel are predictions by the GSWM-09 model. As noted above, estimates are not shown at the lowest or highest altitudes when uncertainties are large or amplitude variations with altitude appear excessive.

[18] Clearly seen in the daily cross sections in Figure 3 are amplitudes and temporal variability similar to those reported earlier over SAAMER by F10a. Figure 3 indicates relatively small amplitudes in general, with maxima of  $\sim 10 \text{ ms}^{-1}$  intermittently occurring primarily at the highest altitudes. Monthly mean amplitudes and phases for DrAAMER and SAAMER shown together in Figure 7 reveal reasonable agreement between the two radars and between 2010 and 2011, within  $\sim 2 \text{ ms}^{-1}$  or less, except where amplitudes are small. The largest departures are seen in June, where amplitude estimates over DrAAMER of  $\sim 1 \text{ ms}^{-1}$  are as much as  $\sim 5 \text{ ms}^{-1}$  less than over SAAMER.

[19] Comparing our observations with GSWM-09 predictions at  $57^\circ\text{S}$ ,  $65^\circ\text{W}$  (approximately midway between SAAMER and DrAAMER), we see that amplitude predictions agree very well, in general, with measurements at both radars. Departures include slight underestimates of measured amplitudes in the zonal component at higher altitudes during April and underestimates of both components at central altitudes during May. GSWM-09 amplitude predictions are typically within the standard deviations of individual monthly estimates except for the underestimates at the highest altitudes during April. Phase predictions by GSWM-09 agree well with measurements over DrAAMER during April in both years up to  $\sim 95 \text{ km}$ , but exhibit phase delays of several hours at middle and higher altitudes compared to SAAMER measurements in both years. GSWM-09 phase predictions are likewise delayed relative to measurements by  $\sim 3\text{--}5 \text{ h}$  during May and  $\sim 5\text{--}10 \text{ h}$  during June, except where amplitudes are too small to allow confident phase estimates.

#### 4.2. Semidiurnal Tide

[20] Time-height cross sections of daily semidiurnal tide zonal and meridional amplitudes over DrAAMER during April, May, and June 2011 are displayed in Figure 3 (bottom left) and 3 (bottom right), respectively. Similar data for 2010 are not shown due to five  $\sim 3$  to 10 day data gaps that preclude a complete analysis of the short-term variability of these motions. Time-height cross sections of daily semidiurnal tide zonal and meridional amplitudes Figures 3 (left) and 3 (right), over SAAMER during April, May, and June of 2009 (Figure 8, top), 2010 (Figure 8, middle), and 2011 (Figure 8, bottom) are displayed for comparison with measurements over DrAAMER. Because of the high correlation between temporal variations of the semidiurnal tides over SAAMER and DrAAMER during 2011, these fields illustrate the intra-annual and interannual variability of the semidiurnal tides over both radars spanning the maximum response occurring in May of each year (see F10a). S transforms of the daily semidiurnal tide amplitudes over SAAMER for each year are shown in Figures 9a–9c and Figures 9e–9g, with those over DrAAMER for 2011 shown in Figures 9d and 9h. Monthly mean semidiurnal tide amplitudes and phases over DrAAMER and SAAMER (red and blue, respectively) are shown together for April (Figure 10, top), May (Figure 10, middle), and June (Figure 10, bottom). As for the diurnal tide in Figure 7, zonal and meridional components are shown at left and right, and results for 2010 and 2011 are shown with solid and dashed lines, respectively. Black lines in each panel are predictions by the GSWM-09 model.

[21] The daily amplitude cross sections in Figure 8 exhibit broad maxima extending from  $\sim$ mid April to mid June

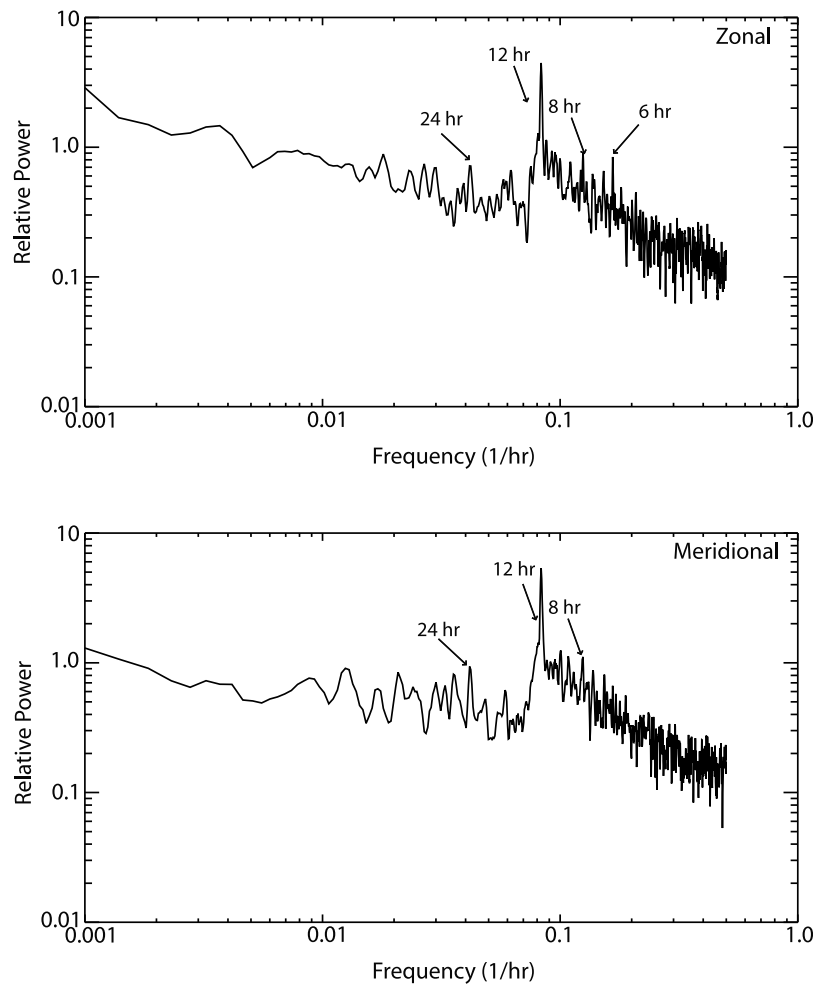


**Figure 6.** Power spectra of hourly (top) zonal and (bottom) meridional winds during April, May, and June 2011 over DrAAMER. Tidal peaks are indicated, and periods are shown from 2 h to  $\sim 40$  days.

each year, meridional amplitudes typically exceeding zonal amplitudes, and significant intra and interannual variability in these responses. For example, meridional amplitudes exceeding  $60 \text{ ms}^{-1}$  extend from  $\sim$ mid April to mid June in 2009 but are largely confined to  $\sim$ mid April to mid May in 2010 and 2011. Notable, however, is the very high correlation between the daily semidiurnal responses over SAAMER and DrAAMER during 2011 displayed in Figures 3 (bottom) and 8 (bottom). In all cases, maximum responses occur at the highest altitudes and approach amplitudes of  $\sim 70 \text{ ms}^{-1}$ . Also seen on examination of Figures 2 and 8 is a tendency for semidiurnal tide amplitudes to be significantly anticorrelated with the corresponding mean winds (zonal and meridional tide amplitude maxima appear correlated with more westward or southward mean winds, respectively). This tendency is seen both for shorter-duration maxima in the zonal component and for more extended intervals in the meridional component, with the latter more conspicuous in the cross sections.

[22] Temporal variability of semidiurnal tide amplitudes discussed in connection with Figures 3 and 8 is quantified with S transforms of these data in Figure 9. Comparing the tidal results in Figure 9 with the mean wind S transforms in

Figure 4, we see much more significant correlations between tidal components exhibiting specific periodicities from  $\sim 5$  to 20 days, as expected given the shorter intrinsic time scales of the tides compared to PWs. As described by F10a, tidal amplitudes exhibit significant variability at expected PW periods as well as longer-period oscillations, and the dominant periodicities are typically seen to occur nearly simultaneously in both tidal components. This is also seen to be the case over the three months during which the semidiurnal tide achieves its maximum amplitudes throughout the year. Examples of strong correlations at specific periodicities include (1) the two maxima at  $\sim 10$  to 12 and 20 days in early April 2009; (2) the maxima at  $\sim 7$  to 8 days in mid to late May and June 2009; (3) the  $\sim 10$  to 12 day maxima in late April 2010; (4) the maxima at  $\sim 12$  to 15 days throughout June 2010; and (5) the multiple maxima at  $\sim 8$  to 15 days in late May and early June 2011 apparently following longer periods at earlier times.

[23] Clear correlations between tides over SAAMER and DrAAMER during 2011 are seen at periods of  $\sim 5$  to 8 days in April and early May and from  $\sim 8$  to 20 days in late May and June. Each of the maxima suggest significant tidal modulation by, or interactions with, the corresponding PW.

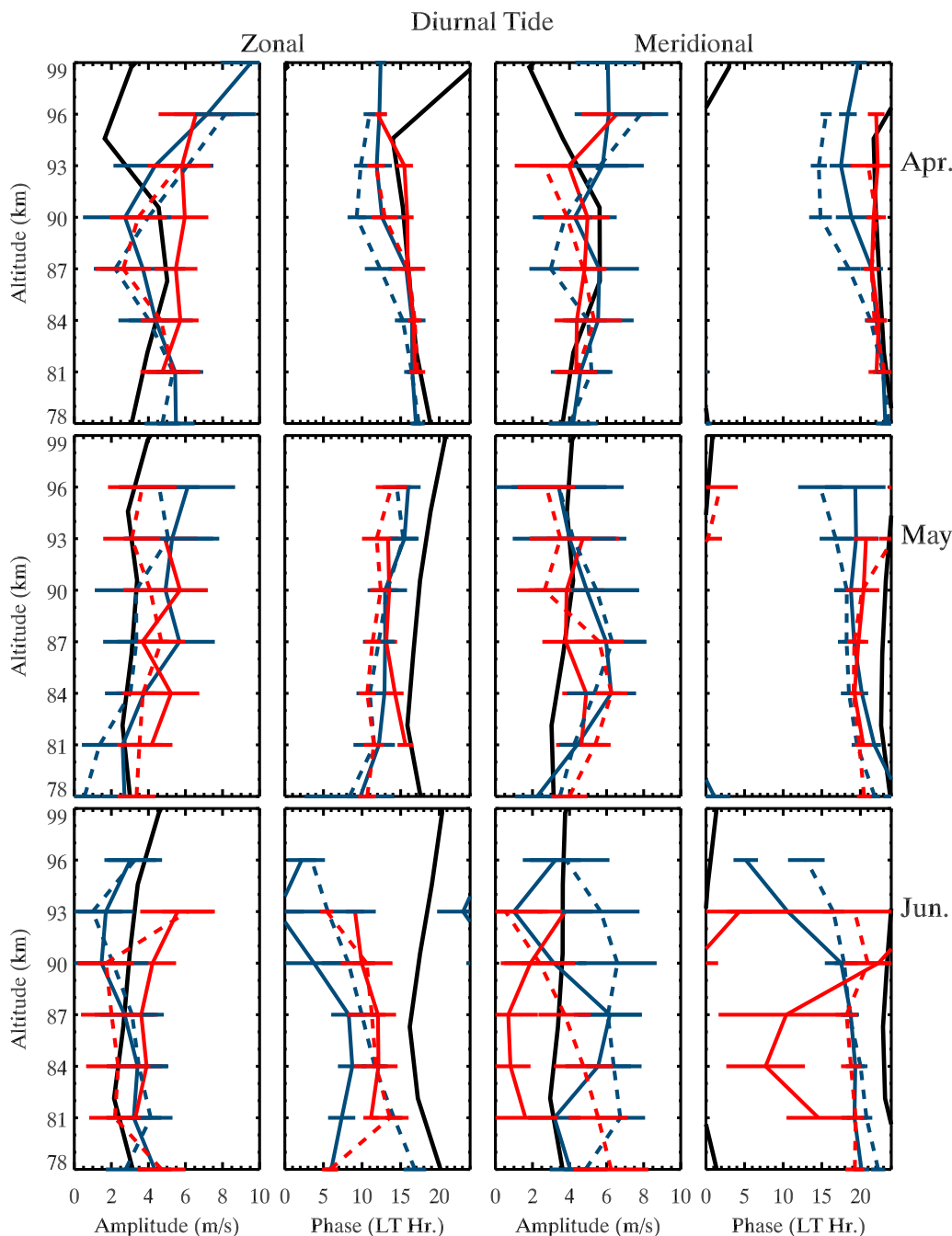


**Figure 7.** Diurnal tide zonal (first column) and meridional (third column) amplitudes and zonal (second column) and meridional (fourth column) phases for (top) April, (middle) May, and (bottom) June of 2010 (solid lines) and 2011 (dashed lines) over DrAAMER (red) and SAAMER (blue). Standard deviations are shown with horizontal lines in each case. Black lines show GSWM-09 predictions.

[24] What is not seen in Figure 9 is evidence of strong tidal amplitude modulation when these amplitudes are largest. Note, for example, that the peaks in the S transforms of semidiurnal tide amplitudes shown in Figure 9 occur in all cases where tidal amplitudes are small. The lack of maxima in the S transforms of tidal amplitudes implies a lack of variability, not small tidal amplitudes. Instead, S transform peaks accompany growth or decay of tidal amplitudes, and suggest that PW interactions may play key roles at these times.

[25] Monthly mean semidiurnal tide amplitudes and phases over DrAAMER and SAAMER shown together in Figure 10 reveal close agreement between the two radars each year and between 2010 and 2011, in most cases. Amplitudes typically increase by factors of  $\sim 3$  from 78 to 99 km in April and May of each year, with a cessation of growth with altitude above  $\sim 90$  km during June of each year. Amplitude profiles are nearly identical for both radars and both years in April, while phases agree between radars, but differ by  $\sim 5$  h between 2010 and 2011. Amplitudes in May and June agree better in

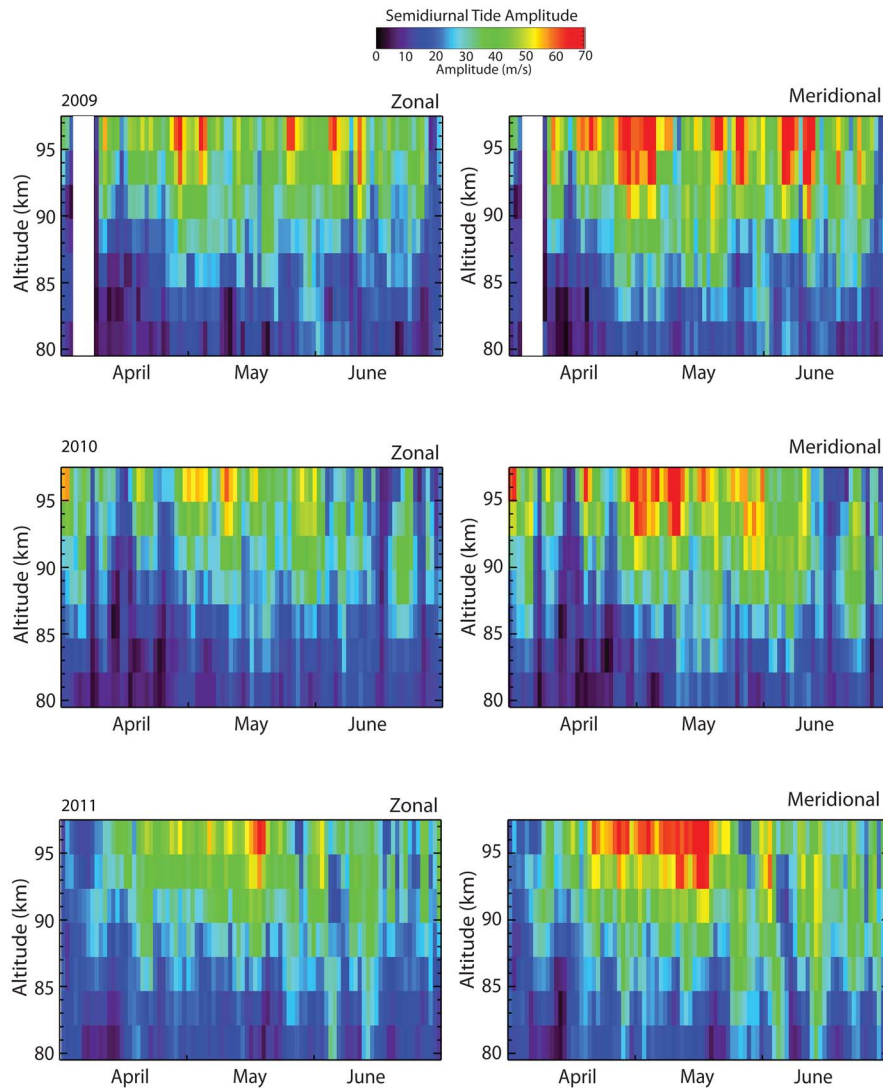


**Figure 8.** As in Figure 2, but for semidiurnal tide amplitudes. Missing data are shown as white.

the two years over each radar, but are  $\sim 20$  to  $50\%$  larger over SAAMER than over DrAAMER each year. Unlike phases in April, those in May and June are in close agreement for both radars and years, except at the lowest altitudes during May where amplitudes are very small. The distinct seasonal maximum over SAAMER in May noted by F10a is seen to also occur over DrAAMER, though with a slightly weaker and lower maximum amplitude in each component.

[26] Comparing our semidiurnal tide observations with GSWM-09 predictions at  $57^\circ\text{S}$ ,  $65^\circ\text{W}$  (as above), we see that amplitude predictions agree very well during April below  $\sim 90$  km, with observed amplitudes larger by  $\sim 30$  to  $50\%$  at higher altitudes. In contrast, GSWM-09 predictions are typically  $\sim 3$  to  $5$  times smaller than observed amplitudes during May and June. They are also smaller than the GSWM-09 predictions in April, while observed amplitudes are larger, except during June at the highest altitude. GSWM-09 predictions of semidiurnal tide phases differ dramatically from our observations during April and May, being more nearly in antiphase than in phase at both sites, despite the significant

phase differences between years during April. GSWM-09 predictions are, however, in reasonable agreement with measurements at both radars during June up to  $\sim 90$  km, above which they diverge and lead observations by  $\sim 4$  h at 99 km.

## 5. GW Momentum Fluxes

[27] Monthly mean GW momentum fluxes over the two radars are displayed in Figure 11. The various panels show zonal and meridional fluxes (left and right) over DrAAMER and SAAMER (red and black) for April (Figure 11, top), May (Figure 11, middle), and June (Figure 11, bottom) of 2010 and 2011 (solid and dashed lines), respectively. Momentum fluxes are shown from 79.5 to 91.5 km, as we have less confidence in momentum flux estimates where meteor counts are small and at the highest altitudes because large semidiurnal tides may introduce significant uncertainties.

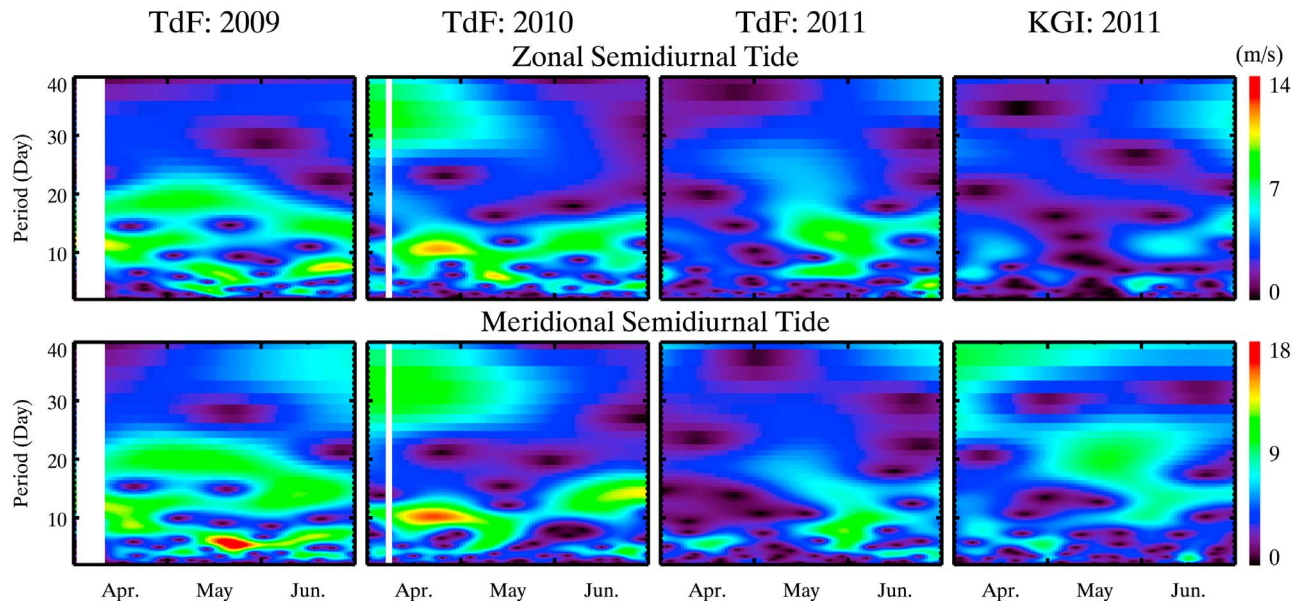


**Figure 9.** As in Figure 4, but for semidiurnal tide amplitudes. Missing data are shown as white.

[28] Monthly mean momentum fluxes displayed in Figure 11 exhibit considerable consistency between 2010 and 2011 at altitudes of 91.5 km and below, within the expected uncertainties of these measurements of  $\sim 10 \text{ m}^2 \text{ s}^{-2}$  assessed by F10b. Zonal momentum fluxes are all close to zero over the 79.5 to 91.5 km altitude range, with estimates for both radars at most times spread nearly symmetrically about zero, again within the expected uncertainties. Meridional momentum fluxes, in contrast, exhibit consistency between 2010 and 2011 and apparently systematic variations from April to June of each year. Meridional momentum fluxes over SAAMER increase from relatively small values of  $\sim 10$  to  $20 \text{ m}^2 \text{ s}^{-2}$  at 79.5 km in these months each year in altitude and with time, with mean values for 2010 and 2011 of  $\sim 20$ ,  $30$ , and  $40 \text{ m}^2 \text{ s}^{-2}$  at 91.5 km. Similar increases are seen to occur over DrAAMER at the higher altitudes (reaching  $\sim 50 \text{ m}^2 \text{ s}^{-2}$  at 91.5 km in June), but with momentum fluxes at the lowest altitudes decreasing from near zero in April to  $\sim -20 \text{ m}^2 \text{ s}^{-2}$  in June.

[29] Zonal momentum fluxes shown in Figure 11 are too close to zero and without clear trends (within our expected uncertainties) to provide useful guidance on the potential GW sources and filtering processes influencing zonal GW propagation at these altitudes. Meridional momentum fluxes, however, are sufficiently nonzero to provide some useful guidance. At lower altitudes, increasingly negative momentum fluxes over DrAAMER from April to June suggest either (1) increasing sources of GWs propagating to the south below  $\sim 85$  km and/or (2) more favorable filtering conditions enabling increasing southward propagation with time. At the higher altitudes, meridional momentum fluxes over DrAAMER and SAAMER increase northward with time, suggesting a prevalence of GWs propagating northward at  $\sim 85$  km and above over both sites. Taken together, these results suggest increasing sources of GWs propagating meridionally over the Drake Passage during April, May, and June of each year, with other dynamics somehow removing

the southward propagating GWs from the spectrum at  $\sim 85$  km and above or enhancing the GWs propagating northward at these altitudes.

## 6. Discussion

### 6.1. Mean Winds

[30] Mean winds observed over DrAAMER and SAAMER during April to June of 2010 and 2011 discussed above are generally consistent with our previous measurements over SAAMER (F10a, F11) and with other assessments of inter-hemispheric mean winds at high latitudes [Avery *et al.*, 1989; Portnyagin *et al.*, 2004, 2006; Dowdy *et al.*, 2007]. In particular, monthly mean zonal winds approaching winter are more strongly eastward over DrAAMER and SAAMER at higher altitudes than at comparable northern latitudes. Monthly mean meridional winds are near zero or weakly poleward throughout our current observations, except over both radars during June 2010, where weakly positive winds ( $< 3 \text{ ms}^{-1}$ ) were observed below  $\sim 90$  km. These interannual fluctuations are nevertheless within the range of variability imposed by PW and longer-period modulations of these monthly means over both radars. The systematically stronger monthly mean zonal winds at these locations, however, appear to be a consequence of the unique large-scale dynamics accompanying the Drake Passage “hotspot” of enhanced GW activity discussed at length by F10a and F10b and references cited above.

### 6.2. Diurnal Tide

[31] Diurnal tide assessments in the present study have addressed only comparisons between sites and interannual comparisons during April to June of 2010 and 2011. We can nevertheless report on improvements in comparisons of current amplitude measurements with the newer GSWM-09 model compared to GSWM-02 predictions. Our previous analysis by F10a compared SAAMER measurements with

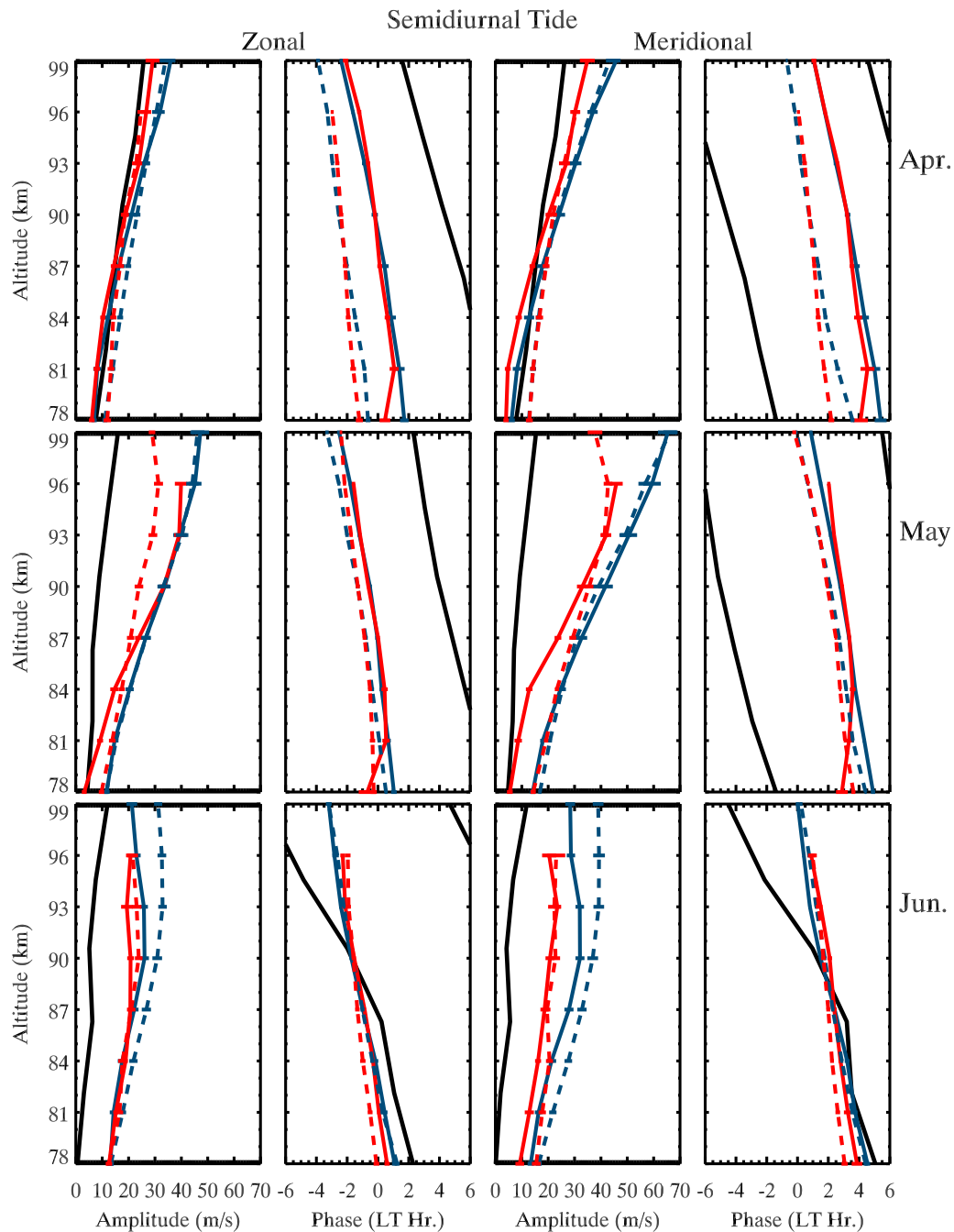


**Figure 10.** As in Figure 7, but for the semidiurnal tide.

GSWM-02 results and found GSWM-02 to systematically overestimate diurnal tide amplitudes over SAAMER. However, current diurnal tide amplitude estimates over DrAAMER and SAAMER are in excellent agreement with GSWM-09 predictions at all but the highest altitudes (95 km and above), due to reductions in the GSWM-09 amplitudes relative to GSWM-02. Measured diurnal tide phases during April to June do not agree as well as the GSWM-02 predictions, however, with systematic delays of predicted wind maxima relative to our radar observations at both sites even at lower altitudes where previous comparisons with SAAMER were very good (see Figure 7 and F10a, Figure 9).

### 6.3. Semidiurnal Tide

[32] Semidiurnal tide assessments in the present analysis are largely consistent with our previous study employing SAAMER (F10a) in which annual maxima of monthly mean semidiurnal tide amplitudes were found to occur in May of each year. Significant interannual variability is also apparent, however, as the monthly mean diurnal amplitudes in the present study over SAAMER are seen to vary from somewhat larger than during 2008 and 2009 to significantly smaller (compare Figure 10 with F10a, Figure 11). Specifically, amplitudes at 99 km during April 2010 and 2011 are  $\sim 10 \text{ ms}^{-1}$  smaller than previous years, amplitudes at 99 km

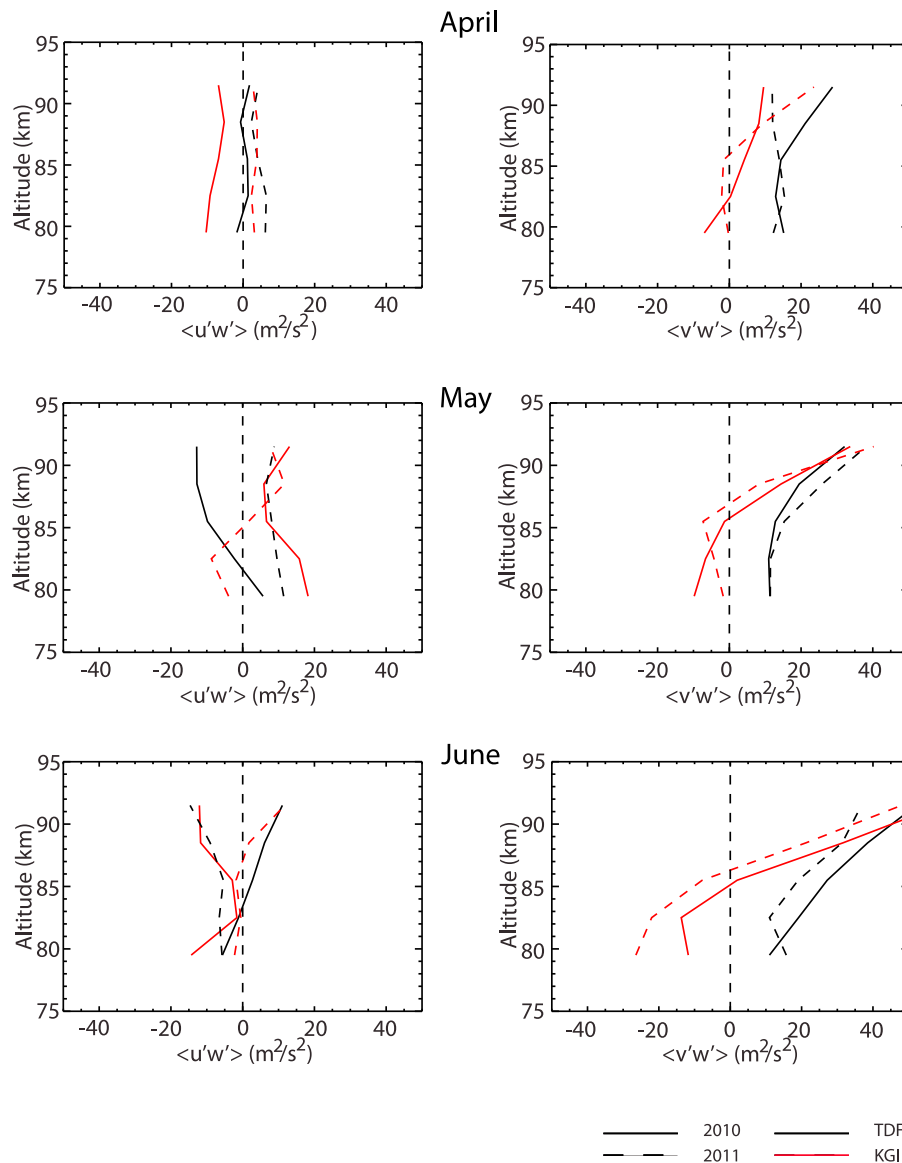


**Figure 11.** Monthly mean (left) zonal and (right) meridional GW momentum fluxes for (top) April, (middle) May, and (bottom) June of (solid lines) 2010 and (dashed lines) 2011 over (red) DrAAMER and (black) SAAMER.

during May are comparable to previous years, while those during June are  $\sim 20$  and  $10 \text{ ms}^{-1}$  smaller than reported by F10a in 2010 and 2011, respectively.

[33] Monthly mean semidiurnal tide amplitudes are systematically smaller over DrAAMER than over SAAMER during April, May, and June 2010 and 2011, with differences of  $\sim 5$  to  $20 \text{ ms}^{-1}$ , though the vertical profiles and phase structures are in close agreement each year. They appear to be similar, however, to those seen in the study of GW-tidal interactions employing the meteor radar at Rothera ( $67.6^\circ\text{S}$ ,  $68.1^\circ\text{W}$ ) by *Beldon and Mitchell* [2010], from which we inferred May 2007 monthly mean zonal and meridional amplitudes at  $\sim 97 \text{ km}$  from composite-day winds to be  $\sim 45$  and  $35 \text{ ms}^{-1}$  (see their Figure 7), respectively.

[34] Also noted in our examination of semidiurnal tide variability were (1) tendencies for amplitudes to achieve maxima during times for which zonal and meridional winds

were minimum (more westward and southward, respectively) and (2) tendencies for the major modulations of the semidiurnal tide at times at which amplitudes were relatively small.

#### 6.4. GW Momentum Fluxes

[35] GW momentum fluxes reported here span April, May, and June 2010 and 2011 over DrAAMER and SAAMER, both of which are within the Drake Passage “hotspot” of GW activity seen during Austral winter to host the strongest stratospheric GW temperature variances observed at any site on Earth [*Jiang et al.*, 2002, 2006; *Eckermann et al.*, 2006]. F10b observed GW momentum fluxes in the MLT over SAAMER during November 2008 and March 2009 that exhibited anticorrelations with mean zonal winds that were consistent with observations at other sites ranging from middle to high latitudes, including the MF radar in Australia [*Vincent and Reid*, 1983; *Reid and Vincent*, 1987; *Fritts and*

Vincent, 1987], the former Poker Flat radar in Alaska [Fritts and Yuan, 1989; Wang and Fritts, 1990, 1991], and the MU radar in Japan [Tsuda et al., 1990]. During Austral winter (June 2008 and 2009 and September 2008), however, zonal momentum fluxes over SAAMER reported by F10b were more nearly correlated with the mean zonal wind, and meridional momentum fluxes were likewise large and positive, suggesting GW propagation eastward and northward away from the Drake Passage at these times.

[36] F10b attributed the November 2008 and March 2009 anticorrelations of momentum fluxes and mean zonal winds to the same GW filtering dynamics believed to account for these correlations at other sites. The unusual relations between momentum fluxes and mean winds (including the larger sustained eastward winds during Austral winter extending to higher altitudes than seen at other sites, with corresponding poleward mean meridional winds occurring at higher altitudes, see F11) were attributed instead to the unique (but poorly understood) dynamics of the Drake Passage “hotspot” and indications of a spectrum of GW sources including jet streams with high eastward winds that might account for eastward GW phase speeds extending into the MLT.

[37] Our present DrAAMER and SAAMER observations are generally consistent with this same picture of the MLT GW and mean flow dynamics. June 2010 and 2011 zonal momentum fluxes are near zero at both sites, thus smaller than estimated over SAAMER in June 2008 or 2009, but comparable to those in March 2009. Mean zonal winds over SAAMER in June 2010 and 2011, however, are somewhat larger than seen over SAAMER in June 2008 and 2009 (by  $\sim 10 \text{ ms}^{-1}$ ). If filtering arguments are relevant to these dynamics, we would expect that stronger eastward winds should contribute to the dissipation of GWs propagating eastward, thus reducing eastward momentum fluxes relative to westward momentum fluxes and causing the net zonal momentum flux to decrease, as seen in our current observations.

[38] If a strong polar night jet at lower altitudes over the Drake Passage contributes GWs having both significant eastward phase speeds and a range of propagation directions (as we expect from spatially localized jet stream forcing), then we should also expect that these GWs will contribute to net northward propagation (and positive meridional momentum fluxes) over SAAMER and net southward propagation (and negative meridional momentum fluxes) over DrAAMER at higher altitudes, apart from additional filtering effects. Such a source would seem to provide an explanation for the positive momentum fluxes over SAAMER and the negative momentum fluxes over DrAAMER below  $\sim 85 \text{ km}$ . At present, however, we have no explanation for why GW momentum fluxes should be positive over the two sites at the northern and southern sides of the Drake passage above  $\sim 85 \text{ km}$ , although auroral heating is one possible source.

[39] As noted by F10b, large GW momentum fluxes accompanying tidal modulation [Fritts and Vincent, 1987; Wang and Fritts, 1991; Espy et al., 2004], arising from specific sources [Espy et al., 2006; Smith et al., 2009], or having no identified cause [Fritts et al., 2002] readily occur in the MLT. Momentum fluxes accompanying such events can significantly exceed the mean values reported at various sites, occasionally by one or two decades. So it is not

surprising that large monthly mean GW momentum fluxes can also occur in regions of demonstrated strong local GW sources, as appears to be the case over DrAAMER and SAAMER, especially during austral winter when multiple strong sources are expected to occur. What remains to be explained are the dynamics that lead to the large mean momentum fluxes observed over the Drake Passage “hotspot” and their implications for the local and global structure and variability of the MLT in this region.

## 7. Summary and Conclusions

[40] We described in this paper a new meteor radar, the Drake Antarctic Agile Meteor Radar (DrAAMER) located at Ferraz Station on King George Island ( $62.1^\circ\text{S}$ ,  $58.7^\circ\text{W}$ ), which, like its predecessor SAAMER located at Rio Grande on Tierra del Fuego ( $53.8^\circ\text{S}$ ,  $67.8^\circ\text{W}$ ), was designed to enable high-resolution wind measurements for assessments of mean, PW, and tidal wind fields, a capability for assessing GW momentum fluxes, and advanced meteor studies. DrAAMER was installed and became operational in March 2010.

[41] To evaluate DrAAMER performance and begin to characterize the large- and smaller-scale dynamics of the Drake Passage “hotspot” more fully, we also described the mean and tidal wind fields and GW momentum flux estimates over DrAAMER during April, May, and June of 2010 and 2011, performed comparisons with correlative measurements by SAAMER, and compared tidal wind measurements at both sites with the newer GSWM-09 model.

[42] Daily mean zonal and meridional winds were found to agree closely between the two sites during April, May, and June 2011 for which correlative data were available. They were also found to exhibit similar structure and variability as seen during 2008 and 2009 over SAAMER. S transforms of these winds revealed dominant periodicities at both sites corresponding to various PW and longer-period oscillations. Primary responses were seen at  $\sim 5$  to 15 days throughout the 3 month data set,  $\sim 20$  to 30 days at the beginning and end of the data set, and  $\sim 30$  to 45 days in the latter portion of the data set. These various responses were somewhat correlated between sites and somewhat stronger in the zonal wind over SAAMER. There was also variability, however, suggesting a delayed response at one site relative to the other or a significant response in one wind component that had a small or no response in the other component. Both the daily mean wind cross sections and their S transforms for SAAMER revealed significant interannual variability in the 3 month interval examined each year.

[43] Monthly mean winds were seen to agree closely between sites, with maximum differences of  $\sim 5 \text{ ms}^{-1}$ . Differences are expected in both the zonal and meridional mean winds at high latitudes, as the zonal jet must decrease toward the pole, and the mean meridional circulation is determined by latitudinally varying GW forcing of the MLT. However, other factors also appear to contribute to the differences observed in our study. These include (1) the large PW and longer-period oscillations seen in the daily mean winds, (2) the lack of exact phasing of these various modulations at the two sites, and (3) data gaps, especially for DrAAMER during 2010, which presumably cause incomplete averaging over the various oscillations influencing each monthly mean.

[44] Tides, especially the semidiurnal tide, are seen to make dominant contributions to the large-scale wind fields. The diurnal tide contributes winds typically of  $\sim 5 \text{ ms}^{-1}$  at most altitudes, with maxima approaching  $\sim 10 \text{ ms}^{-1}$ , except at the highest altitudes where daily amplitudes may be twice as large. Semidiurnal tide zonal and meridional winds, in contrast, contribute very significantly to the motion field over both radars, with monthly mean amplitudes typically approaching  $\sim 20$  to  $50 \text{ ms}^{-1}$  at the highest altitudes, with maxima of  $\sim 65 \text{ ms}^{-1}$  in the meridional component over SAAMER in June and daily amplitudes exceeding  $\sim 70 \text{ ms}^{-1}$ . Semidiurnal tide amplitudes are typically  $\sim 20\%$  to  $50\%$  larger over SAAMER than over DrAAMER each year. They also tend to be anticorrelated with eastward and northward winds and to exhibit the greatest variability at various PW periods when amplitudes are small.

[45] Our limited analysis also suggests little interannual variability of monthly mean semidiurnal tide amplitudes over SAAMER during April and May and over DrAAMER during April and June of 2010 and 2011, with greater interannual variability over DrAAMER during May and at lower altitudes, and over SAAMER during June. Semidiurnal phases compare closely between the two sites in both components each year, but exhibit greater interannual variability in April than in May or June (phase differences of  $\sim 2$  to  $3 \text{ h}$  in April and  $\sim 1 \text{ h}$  or less in May and June). Phase progression is downward and relatively uniform in altitude, implying upward propagation and a vertical wavelength of  $\sim 60$  to  $80 \text{ km}$ . Semidiurnal tide amplitudes are systematically larger than predictions by the GSWM-09 model, with the largest discrepancies occurring in May and June. Significant phase discrepancies are also observed, being more nearly in anti-phase during April and May, but in phase below  $\sim 90 \text{ km}$  in June, with departures increasing at higher altitudes implying a shorter predicted vertical wavelength than observed.

[46] Our analysis of GW momentum fluxes during April, May, and June 2010 and 2011 revealed significant consistency between sites and years, as well as with the general findings by F10b over SAAMER in 2008 and 2009, but significant departures from mean wind and momentum flux correlations widely reported elsewhere and also seen over SAAMER except in Austral winter. These differences were attributed to the expected unique (but poorly understood) dynamics of the Drake Passage “hotspot” and indications of a spectrum of GW sources including jet streams with high eastward winds that might account for eastward GW phase speeds extending into the MLT and the stronger eastward mean winds in this region than seen at comparable northern latitudes. Our inferred GW momentum fluxes exhibited zonal mean values near zero (within our estimation uncertainties), suggesting a balance between eastward and westward GW momentum transport that is consistent with the lack of significant zonal mean wind variations with altitude. Significant differences were seen in the mean meridional momentum fluxes over SAAMER and DrAAMER, with negative and positive fluxes, respectively, below  $\sim 85 \text{ km}$  approaching Austral winter, and positive fluxes over both radars at higher altitudes. The momentum flux variations at lower altitudes were considered to be consistent with possible jet stream sources primarily over the Drake Passage, with dominant GW propagation northward and southward over SAAMER and DrAAMER, respectively.

[47] We have no explanation at present for the increasing positive meridional momentum fluxes at higher altitudes, and the corresponding implied equatorward GW propagation. Auroral GW generation is one possibility, but there are no measurements of momentum fluxes in polar winter at these altitudes (even the Poker Flat radar was unable to make measurements in winter above  $\sim 85 \text{ km}$ ), nor are there modeling studies that predict GW responses to auroral forcing. Thus, an explanation will need to await further quantification of these dynamics.

[48] **Acknowledgments.** Research described in this paper was performed under NSF grants OPP-0839084 and ATM-0634650. We are especially grateful to the Secretaria for the Interministerial Commission of Sea Resources (SECIRM), the Brazilian Antarctic Program (PROANTAR), the National Institute for Science and Technology, Antarctic Environmental Research (INCT-APA), and the ATMANAR/MCT/CNPq project, FAPERJ, for their support of this research and visits to Ferraz Station to install and service DrAAMER. We are also very grateful for the valuable assistance of personnel at Estacion Astronomica Rio Grande (EARG) with the operations and maintenance of SAAMER. J. V. Bageston thanks FAPESP for his postdoctorate fellowship under the process number 2010/06608-2. Finally, we are indebted to MARDOC and Genesis Software for working with us to devise a radar configuration that met our measurement objectives. We also acknowledge use of the CEDAR database and the GSWM-09 website at NCAR for GSWM-09 results employed for our comparisons.

## References

- Alexander, M. J., et al. (2008a), Global estimates of gravity wave momentum flux from high resolution dynamics limb sounder observations, *J. Geophys. Res.*, *113*, D15S18, doi:10.1029/2007JD008807.
- Alexander, M. J., H. Teitelbaum, S. D. Eckermann, J. Gille, J. Barnett, and C. Barnet (2008b), High-resolution satellite observations of mountain waves, *Bull. Am. Meteor. Soc.*, *89*, 151–152.
- Avery, S. K., R. A. Vincent, A. Phillips, A. H. Manson, and G. J. Fraser (1989), High-latitude tidal behavior in the mesosphere and lower thermosphere, *J. Atmos. Terr. Phys.*, *51*(7–8), 595–608, doi:10.1016/0021-9169(89)90057-3.
- Beldon, C. L., and N. J. Mitchell (2010), Gravity wave–tidal interactions in the mesosphere and lower thermosphere over Rothera, Antarctica ( $68^\circ\text{S}$ ,  $68^\circ\text{W}$ ), *J. Geophys. Res.*, *115*, D18101, doi:10.1029/2009JD013617.
- Burrage, M. D., M. E. Hagan, W. R. Skinner, D. L. Wu, and P. B. Hays (1995), Long-term variability in the solar diurnal tide observed by HRDI and simulated by the GSWM, *Geophys. Res. Lett.*, *22*(19), 2641–2644, doi:10.1029/95GL02635.
- Dowdy, A. J., R. A. Vincent, M. Tsutsumi, K. Igarashi, Y. Murayama, W. Singer, and D. J. Murphy (2007), Polar mesosphere and lower thermosphere dynamics: 1. Mean wind and gravity wave climatologies, *J. Geophys. Res.*, *112*, D17104, doi:10.1029/2006JD008126.
- Eckermann, S. D., and C. J. Marks (1996), An idealized ray model of gravity wave–tidal interactions, *J. Geophys. Res.*, *101*(D16), 21,195–21,212.
- Eckermann, S. D., D. L. Wu, J. D. Doyle, J. F. Burris, T. J. McGee, C. A. Hostetler, L. Coy, B. N. Stephens, J. P. McCormack, and T. F. Hogan (2006), Imaging gravity waves in lower stratospheric AMSU-A radiances, part 2: Validation case study, *Atmos. Chem. Phys.*, *6*, 3343–3362, doi:10.5194/acp-6-3343-2006.
- Em, M., P. Preusse, M. J. Alexander, and C. D. Warner (2004), Absolute values of gravity wave momentum flux derived from satellite data, *J. Geophys. Res.*, *109*, D20103, doi:10.1029/2004JD004752.
- Espy, P. J., G. O. L. Jones, G. R. Swenson, J. Tang, and M. J. Taylor (2004), Tidal modulation of the gravity-wave momentum flux in the Antarctic mesosphere, *Geophys. Res. Lett.*, *31*, L11111, doi:10.1029/2004GL019624.
- Espy, P. J., R. E. Hibbins, G. R. Swenson, J. Tang, M. J. Taylor, D. M. Riggan, and D. C. Fritts (2006), Regional variations of mesospheric gravity wave momentum fluxes over Antarctica, *Ann. Geophys.*, *24*, 81–88.
- Forbes, J. M. (1995), Tidal and planetary waves, in *The Upper Mesosphere and Lower Thermosphere: A Review of Experiment and Theory*, *Geophys. Monogr. Ser.*, vol. 87, edited by R. M. Johnson and T. L. Killeen, pp. 67–88, AGU, Washington D. C.
- Forbes, J. M., J. Gu, and S. Miyahara (1991), On the interactions between gravity waves and the diurnal propagating tide, *Planet. Space Sci.*, *39*, 1249–1257, doi:10.1016/0032-0633(91)90038-C.

- Fritts, D. C., and M. J. Alexander (2003), Gravity dynamics and effects in the middle atmosphere, *Rev. Geophys.*, *41*(1), 1003, doi:10.1029/2001RG000106.
- Fritts, D. C., and R. A. Vincent (1987), Mesospheric momentum flux studies at Adelaide, Australia: Observations and a gravity wave–tidal interaction model, *J. Atmos. Sci.*, *44*, 605–619, doi:10.1175/1520-0469(1987)044<0605:MMFSAA>2.0.CO;2.
- Fritts, D. C., and L. Yuan (1989), Measurement of momentum fluxes near the summer mesopause at Poker Flat, Alaska, *J. Atmos. Sci.*, *46*, 2569–2579, doi:10.1175/1520-0469(1989)046<2569:MOMFNT>2.0.CO;2.
- Fritts, D. C., T. Tsuda, T. E. VanZandt, S. A. Smith, T. Sato, S. Fukao, and S. Kato (1990), Studies of velocity fluctuations in the lower atmosphere using the MU radar: Part II: Momentum fluxes and energy densities, *J. Atmos. Sci.*, *47*, 51–66, doi:10.1175/1520-0469(1990)047<0051:SOVFI>2.0.CO;2.
- Fritts, D. C., S. A. Vadas, and Y. Yamada (2002), An estimate of strong local gravity wave body forcing based on OH airglow and meteor radar observations, *Geophys. Res. Lett.*, *29*(10), 1429, doi:10.1029/2001GL013753.
- Fritts, D. C., et al. (2010a), Southern Argentina Agile Meteor Radar: System design and initial measurements of large-scale winds and tides, *J. Geophys. Res.*, *115*, D18112, doi:10.1029/2010JD013850.
- Fritts, D. C., D. Janches, and W. K. Hocking (2010b), Southern Argentina Agile Meteor Radar: Initial assessment of gravity wave momentum fluxes, *J. Geophys. Res.*, *115*, D19123, doi:10.1029/2010JD013891.
- Fritts, D. C., H. Iimura, R. Lieberman, D. Janches, and W. Singer (2011), A conjugate study of mean winds and planetary waves employing enhanced meteor radars at Rio Grande, Argentina (53.8°S) and Juliusruh, Germany (54.6°N), *J. Geophys. Res.*, doi:10.1029/2011JD016305, in press.
- Hagan, M. E., and J. M. Forbes (2002), Migrating and nonmigrating diurnal tides in the middle and upper atmosphere excited by tropospheric latent heat release, *J. Geophys. Res.*, *107*(D24), 4754, doi:10.1029/2001JD001236.
- Hagan, M. E., and J. M. Forbes (2003), Migrating and nonmigrating semi-diurnal tides in the upper atmosphere excited by tropospheric latent heat release, *J. Geophys. Res.*, *108*(A2), 1062, doi:10.1029/2002JA009466.
- Hagan, M. E., M. D. Burrage, J. M. Forbes, J. Hackney, W. J. Randel, and X. Zhang (1999), GSWM-98: Results for migrating solar tides, *J. Geophys. Res.*, *104*(A4), 6813–6827.
- Hertzog, A., G. Boccara, R. A. Vincent, F. Vial, and P. Cocquerez (2008), Estimation of gravity wave momentum flux and phase speeds from quasi-Lagrangian stratospheric balloon flights. Part II: Results from the Vorcore campaign in Antarctica, *J. Atmos. Sci.*, *65*, 3056–3070, doi:10.1175/2008JAS2710.1.
- Hocking, W. K. (2005), A new approach to momentum flux determinations using SKiYMET meteor radars, *Ann. Geophys.*, *23*, 2433–2439, doi:10.5194/angeo-23-2433-2005.
- Holton, J. R. (1984), The generation of mesospheric planetary waves by zonally asymmetric gravity wave breaking, *J. Atmos. Sci.*, *41*, 3427–3430, doi:10.1175/1520-0469(1984)041<3427:TGOMPW>2.0.CO;2.
- Isler, J. R., and D. C. Fritts (1996), Gravity wave variability and interactions with lower-frequency motions in the mesosphere and lower thermosphere over Hawaii, *J. Atmos. Sci.*, *53*, 37–48, doi:10.1175/1520-0469(1996)053<0037:GWVAIW>2.0.CO;2.
- Jiang, J. H., D. L. Wu, and S. D. Eckermann (2002), Upper Atmosphere Research Satellite (UARS) MLS observation of mountain waves over the Andes, *J. Geophys. Res.*, *107*(D20), 8273, doi:10.1029/2002JD002091.
- Jiang, J. H., S. D. Eckermann, D. L. Wu, and D. Y. Wang (2006), Interannual variation of gravity waves in the Arctic and Antarctic winter middle atmosphere, *Adv. Space Res.*, *38*, 2418–2423, doi:10.1016/j.asr.2005.09.036.
- Jones, J., A. R. Webster, and W. K. Hocking (1998), An improved interferometer design for use with meteor radars, *Radio Sci.*, *33*(1), 55–65, doi:10.1029/97RS03050.
- Lieberman, R. S., J. Oberheide, M. E. Hagan, E. E. Remsberg, and L. L. Gordley (2004), Variability of diurnal tides and planetary waves during November 1978–May 1979, *J. Atmos. Sol. Terr. Phys.*, *66*(6–9), 517–528, doi:10.1016/j.jastp.2004.01.006.
- Liu, X., J. Xu, H.-L. Liu, and R. Ma (2008), Nonlinear interactions between gravity waves with different wavelengths and diurnal tide, *J. Geophys. Res.*, *113*, D08112, doi:10.1029/2007JD009136.
- Lu, W., and D. C. Fritts (1993), Spectral estimates of gravity wave energy and momentum fluxes, III: Gravity wave–Tidal interactions, *J. Atmos. Sci.*, *50*, 3714–3727, doi:10.1175/1520-0469(1993)050<3714:SEOGWE>2.0.CO;2.
- Manson, A. H., C. E. Meek, and G. E. Hall (1998), Correlations of gravity waves and tides in the mesosphere over Saskatoon, *J. Atmos. Solar Terr. Phys.*, *60*, 1089–1107.
- Manson, A. H., et al. (1999), Seasonal variations of the semi-diurnal and diurnal tides in the MLT: Multi-year MF radar observations from 2 to 70°N, and the GSWM tidal model, *J. Atmos. Sol. Terr. Phys.*, *61*, 809–828, doi:10.1016/S1364-6826(99)00045-0.
- McLandress, C. (1998), On the importance of gravity waves in the middle atmosphere and their parameterization in general circulation models, *J. Atmos. Sol. Terr. Phys.*, *60*, 1357–1383, doi:10.1016/S1364-6826(98)00061-3.
- McLandress, C. (2002), The seasonal variation of the propagating diurnal tide in the mesosphere and lower thermosphere. Part I: The role of gravity waves and planetary waves, *J. Atmos. Sci.*, *59*, 893–906, doi:10.1175/1520-0469(2002)059<0893:TSVOTP>2.0.CO;2.
- McLandress, C., and W. E. Ward (1994), Tidal/gravity wave interactions and their influence on the large-scale dynamics of the middle atmosphere: Model results, *J. Geophys. Res.*, *99*, 8139–8155, doi:10.1029/94JD00486.
- McLandress, C., M. J. Alexander, and D. L. Wu (2000), Microwave Limb Sounder observations of gravity waves in the stratosphere: A climatology and interpretation, *J. Geophys. Res.*, *105*(D9), 11,947–11,967, doi:10.1029/2000JD900097.
- Meyer, C. K. (1999), Gravity wave interactions with the diurnal propagating tide, *J. Geophys. Res.*, *104*, 4223–4239, doi:10.1029/1998JD200089.
- Miyahara, S. (1985), Suppression of stationary planetary waves by internal gravity waves in the mesosphere, *J. Atmos. Sci.*, *42*, 100–112, doi:10.1175/1520-0469(1985)042<0100:SOSPWB>2.0.CO;2.
- Miyahara, S., Y. Hayashi, and J. D. Mahlman (1986), Interactions between gravity waves and planetary-scale flow simulated by the GFDL “SKYHI” general circulation model, *J. Atmos. Sci.*, *43*, 1844–1861, doi:10.1175/1520-0469(1986)043<1844:IBGWAP>2.0.CO;2.
- Murphy, D. J., and R. A. Vincent (1998), Mesospheric momentum fluxes over Adelaide during the 2-day wave: Results and interpretation, *J. Geophys. Res.*, *103*, 28,627–28,636, doi:10.1029/1998JD200001.
- Murphy, D. J., et al. (2006), A climatology of tides in the Antarctic mesosphere and lower thermosphere, *J. Geophys. Res.*, *111*, D23104, doi:10.1029/2005JD006803.
- Ortland, D. A., and M. J. Alexander (2006), Gravity wave influence on the global structure of the diurnal tide in the mesosphere and lower thermosphere, *J. Geophys. Res.*, *111*, A10S10, doi:10.1029/2005JA011467.
- Pancheva, D., et al. (2002), Global-scale tidal structure in the mesosphere and lower-thermosphere during the PSMOS campaign of June–August 1999 and comparisons with the global-scale wave model, *J. Atmos. Sol. Terr. Phys.*, *64*, 1011–1035.
- Pancheva, D., et al. (2004), Variability of the quasi-2-day wave observed in the MLT region during the PSMOS campaign of June–August 1999, *J. Atmos. Sol. Terr. Phys.*, *66*, 539–565, doi:10.1016/j.jastp.2004.01.008.
- Pancheva, D., P. Mukhtarov, and B. Andonov (2009), Global structure, seasonal and interannual variability of the migrating semidiurnal tide seen in the SABER/TIMED temperatures (2002–2007), *Ann. Geophys.*, *27*, 687–703, doi:10.5194/angeo-27-687-2009.
- Portnyagin, Y., et al. (2004), Mesosphere/lower thermosphere prevailing wind model, *Adv. Space Res.*, *34*, 1755–1762, doi:10.1016/j.asr.2003.04.058.
- Portnyagin, Y. I., E. G. Merzlyakov, T. V. Solov’eva, and N. A. Makarov (2006), Interhemispheric distinctions in wind-regime parameters in the polar mesosphere-lower thermosphere, *Izv. Russ. Acad. Sci. Atmos. Oceanic Phys., Engl. Transl.*, *42*(1), 93–104, doi:10.1134/S0001433806010099.
- Preusse, P., S. D. Eckermann, J. Oberheide, M. E. Hagan, and D. Offermann (2001), Modulation of gravity waves by tides as seen in CRISTA temperatures, *Adv. Space Res.*, *27*(10), 1773–1778, doi:10.1016/S0273-1177(01)00336-2.
- Preusse, P., A. Dornbrack, S. D. Eckermann, M. Riese, B. Schaeler, J. T. Bacmeister, D. Broutman, and K. U. Grossmann (2002), Space based measurements of stratospheric mountain waves by CRISTA 1. Sensitivity, analysis method and a case study, *J. Geophys. Res.*, *107*(D23), 8178, doi:10.1029/2001JD000699.
- Preusse, P., et al. (2006), Tropopause to mesopause gravity waves in August: Measurement and modeling, *J. Atmos. Sol. Terr. Phys.*, *68*, 1730–1751, doi:10.1016/j.jastp.2005.10.019.
- Reid, I. M., and R. A. Vincent (1987), Measurements of mesospheric gravity wave momentum fluxes and mean flow accelerations at Adelaide, Australia, *J. Atmos. Sol. Terr. Phys.*, *49*, 443–460, doi:10.1016/0021-9169(87)90039-0.
- Smith, S., J. Baumgardner, and M. Mendillo (2009), Evidence of mesospheric gravity waves generated by orographic forcing in the troposphere, *Geophys. Res. Lett.*, *36*, L08807, doi:10.1029/2008GL036936.
- Stockwell, R. G., L. Mansinha, and R. Lowe (1996), Localization of the complex spectrum: The S transform, *IEEE Trans. Signal Process.*, *44*(4), 998–1001, doi:10.1109/78.492555.

- Thayaparan, T., W. K. Hocking, and J. MacDougall (1995), Observational evidence of tidal/gravity wave interactions using the UW0 2MHz radar, *Geophys. Res. Lett.*, *22*(4), 373–376, doi:10.1029/94GL03270.
- Tsuda, T., Y. Murayama, M. Yamamoto, S. Kato, and S. Fukao (1990), Seasonal variation of momentum flux in the mesosphere observed with the MU radar, *Geophys. Res. Lett.*, *17*(6), 725–728, doi:10.1029/GL017i006p00725.
- Tsuda, T., M. Nishida, C. Rocken, and R. H. Ware (2000), A global morphology of gravity wave activity in the stratosphere revealed by the GPS occultation data (GPS/MET), *J. Geophys. Res.*, *105*(D6), 7257–7273, doi:10.1029/1999JD901005.
- VanZandt, T. E., S. A. Smith, T. Tsuda, D. C. Fritts, T. Sato, S. Fukao, and S. Kato (1990), Studies of velocity fluctuations in the lower atmosphere using the MU radar. Part I: Azimuthal anisotropy, *J. Atmos. Sci.*, *47*(1), 39–50, doi:10.1175/1520-0469(1990)047<0039:SOVFIT>2.0.CO;2.
- Vincent, R. A., and I. M. Reid (1983), HF Doppler measurements of mesospheric momentum fluxes, *J. Atmos. Sci.*, *40*, 1321–1333, doi:10.1175/1520-0469(1983)040<1321:HDMOMG>2.0.CO;2.
- Vincent, R. A., S. Kovalam, D. C. Fritts, and J. R. Isler (1998), Long-term MF radar observations of solar tides in the low-latitude mesosphere: Interannual variability and comparisons with the GSWM, *J. Geophys. Res.*, *103*(D8), 8667–8683, doi:10.1029/98JD00482.
- Wang, D.-Y., and D. C. Fritts (1990), Mesospheric momentum fluxes observed by the MST radar at Poker Flat, Alaska, *J. Atmos. Sci.*, *47*, 1512–1521, doi:10.1175/1520-0469(1990)047<1512:MMFOBT>2.0.CO;2.
- Wang, D.-Y., and D. C. Fritts (1991), Evidence of gravity wave-tidal interaction observed near the summer mesopause at Poker Flat, Alaska, *J. Atmos. Sci.*, *48*, 572–583, doi:10.1175/1520-0469(1991)048<0572:EOGWIO>2.0.CO;2.
- Wu, D. L. (2004), Mesoscale gravity wave variances from AMSU-A radiances, *Geophys. Res. Lett.*, *31*, L12114, doi:10.1029/2004GL019562.
- Wu, D. L., and S. D. Eckermann (2008), Global gravity wave variances from Aura MLS: Characteristics and interpretation, *J. Atmos. Sci.*, *65*, 3695–3718, doi:10.1175/2008JAS2489.1.
- Wu, D. L., and J. H. Jiang (2002), MLS observations of atmospheric gravity waves over Antarctica, *J. Geophys. Res.*, *107*(D24), 4773, doi:10.1029/2002JD002390.
- Wu, D. L., P. Preusse, S. D. Eckermann, J. H. Jiang, M. de la Torre Juarez, L. Coy, and D. Y. Wang (2006), Remote sounding of atmospheric gravity waves with satellite limb and nadir techniques, *Adv. Space Res.*, *37*, 2269–2277, doi:10.1016/j.asr.2005.07.031.
- Zhang, X., J. M. Forbes, and M. E. Hagan (2010a), Longitudinal variation of tides in the MLT region: 1. Tides driven by tropospheric net radiative heating, *J. Geophys. Res.*, *115*, A06316, doi:10.1029/2009JA014897.
- Zhang, X., J. M. Forbes, and M. E. Hagan (2010b), Longitudinal variation of tides in the MLT region: 2. Relative effects of solar radiative and latent heating, *J. Geophys. Res.*, *115*, A06317, doi:10.1029/2009JA014898.

---

J. V. Bageston and N. M. P. Leme, Instituto Nacional de Pesquisas Espaciais, Av. dos Astronautas, 1758, São José dos Campos, São Paulo 12227-010, Brazil.

D. C. Fritts and H. Imura, Colorado Research Associates Division, NorthWest Research Associates, 3380 Mitchell Ln., Boulder, CO 80301, USA. (dave@cora.nwra.com)

W. K. Hocking, Department of Physics, University of Western Ontario, 1151 Richmond St., London, ON N6A 3K7, Canada.

D. Janches, Space Weather Laboratory, NASA Goddard Space Flight Center, Code 674, Greenbelt, MD 20771, USA.